ISABE-2011-1242

COMPARISON OF DIFFERENT NUMERICAL APPROACHES AT THE CENTRIFUGAL COMPRESSOR RADIVER

Oliver Borm, Balint Balassa, Hans-Peter Kau

Institute for Flight Propulsion,
Technische Universität München,
Boltzmannstr. 15
D-85748 Garching, Germany
Email: borm@lfa.mw.tum.de

ABSTRACT

This paper presents a comparison of different numerical software packages for the flow simulation of a centrifugal compressor at the example of the RADIVER testcase. Three dimensional steady state numerical simulations have been carried out with the Numeca and OpenFOAM CFD codes. The used turbulence models are Spalart-Allmaras and k-ω SST, which were also coupled with a conjugate heat transfer (CHT) simulation. All simulations are analyzed in the compressor map along with the experiments. The temperature distributions of the CHT simulations are examined and their implications reviewed. The simulations cover three operating points at 80% design speed. One operating point of the fluid simulations near the surge line is compared in detail to the data from experiments conducted on the compressor. Velocity vector components and turbulence intensities are plotted and reviewed. Similarities and differences are discussed and their causes and effects pointed out.

NOMENCLATURE

Latin Symbols

α	absolute flow angle
β	relative flow angle
$\eta_{s,tt}$	isentropic total-total efficiency
$\varkappa$	ratio of heat capacities
λ	heat conductivity
ν_t	turbulent viscosity
Π_{tt}	total-total pressure ratio

Subscripts

Imp	Impeller
t	total
red	value corrected to ISA conditions

Abbreviations

2M	measurement section shortly downstream impeller exit
2M'	measurement section shortly before impeller exit
ALE	Arbitrary Lagrangian Eulerian
$\vec{c}$	absolute velocity
c_p	specific heat capacity at constant pressure
CHT	Conjugate Heat Transfer
ISA	International Standard Atmosphere
L2F	Laser-2-Focus
MRF	Multiple Rotating Reference Frame
p	pressure
PS	Pressure Side
SA	Spalart-Allmaras
SS	Suction Side
SST	Shear-Stress-Transport
T	temperature
$\vec{w}$	relative velocity

INTRODUCTION

Different numerical approaches exist in order to simulate the transonic flow in rotating turbomachinery. They differ in the formulation of the conservation equations, as different source terms may apply. As well as in the formulation of numerical schemes. This leads to diverse results when using different codes for the same problem. It is the purpose of this paper to investigate the behavior of two different density based solvers in comparison to existing experimental results and analyze them in detail.

Ziegler [1] performed extensive experiments with the RADIVER compressor. Measurement probes were used to determine pressure and temperature of the fluid. Furthermore the Laser-2-Focus method was applied to measure the two dimensional fluid velocity vector at different sections of the machine.

For a complete overview of the measurement data sets the reader may refer to [1]. The experimental results are well suited to validate numerical simulations of centrifugal compressors. In this paper the stage with a vaneless diffuser is investigated.

Weiss [2] performed simulations of the stage with vaneless diffuser using the code from his institute. There the influence of the rotor tip gap size as well as the inlet boundary condition were investigated. Furthermore Boncinelli [3] and Smirnov [4] did steady and unsteady simulations. They primarily investigated the rotor stator interaction.

In the case of a CHT simulation, the temperature distribution in fluid and solid is solved simultaneously. At the solid-fluid interface a conservative heat transfer boundary condition is applied.

Solver Description

The Fine/Turbo solver from Numeca is based on a central scheme. As default, a relative velocity formulation for rotating machinery is used. The transonicMRFDyMFoam solver is based on an upwind scheme (HLLC) and was developed by Borm [5] inside the CFD Toolbox OpenFOAM-extend. Nevertheless for convenience reasons, the presented simulations and results are in the following only referred to as OpenFOAM. For Multiple Rotating Reference Frames (MRF) an Arbitrary Lagrangian Eulerian (ALE) type formulation was chosen in OpenFOAM, which is based on the absolute velocity.

Both solvers are formally of second order accuracy. Numeca Fine/Turbo uses additional matrix dissipation terms in order to avoid spurious oscillations near strong gradients, while the OpenFOAM solver uses a slope limiter for the same reason. The multidimensional Venkatakrishnan slope limiter with a constant of $C = 5$ was used in all the presented OpenFOAM simulations .

For both solvers the default k-ω SST turbulence model was chosen. As there are several formulations of this model, and also the near wall treatment might be different in both CFD codes, one could not make sure that these two models are identical. Moreover local time stepping was used in both solvers for a faster convergence.

Numerical Model

Geometry

The RADIVER compressor stage consists of an impeller and a wedge type diffuser. The vaned diffuser can take different configurations. In this case only the vaneless diffuser was investigated. The geometry as well as construction drawings were published by Ziegler [1].

The impeller has 15 blades and a trailing edge radius of 135 *mm*. The rotational speed in the computations and experiments is 28160 rpm which is 80% of the design speed and equivalent to a circumferential velocity of 398.1 $\frac{m}{s}$ at the trailing edge. The vanless diffuser has a constant span of $b = 11.1$ *mm* and the outlet is located at a radius of $r_8 = 345$ *mm*.

Measurement Positions

Several measurement sections were placed at interesting meridional positions in the experiments. This paper however focuses on the positions 2M and 2M', because they show the most relevant data of the impeller flow.

The 2M cylindrical surface is positioned shortly downstream the impeller at a radius of $r_{2M} = 139$ *mm*. The 2M' measurement section is located shortly before the end of the impeller channel and is enclosed on each side by the rotor blades. It intersects with the shroud at $r_{2M'} = 133.8$ *mm* and has a pitch to the machine axis of $\gamma = 4.672°$, as shown in Fig. 1. This way the measurement section forms a part of a cone surface.

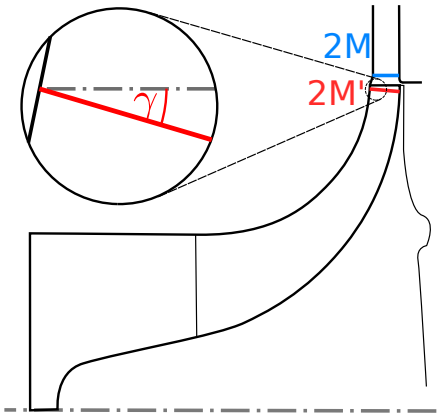

Figure 1. Relevant measurement sections

Mesh

The used meshes can be divided in three geometrical parts. One mesh each for the fluid in the impeller, for the fluid in the vaneless diffuser and for the solid hub in the case of CHT computations. Two different sized fluid meshes were created. All meshes have a sufficient cell and face quality in terms of aspect ratio, expansion ratio, skewness and non-orthogonality.

Fine Mesh The fine fluid mesh was used within Numeca and OpenFOAM simulations. It consists of an impeller mesh with 1.22 million cells and was generated with Numeca AutoGrid. It is based on an OH mesh topology and has a non matching boundary condition in the tip gap between pressure and suction side. The periodic boundary conditions match exactly this way. The block structured impeller mesh was converted with cgnsToFoam into an OpenFOAM compatible format. The rotor tip gap

at leading edge ($s_1 = 0.7\ mm$) and trailing edge ($s_2 = 0.48\ mm$) published by Weiss [2] was used in AutoGrid for both impeller meshes. The interpolation of this tip gap height between leading and trailing edge was done by AutoGrid automatically.

The vaneless diffuser mesh was created by blockMesh from OpenFOAM and consists of 322k cells. Each block of this mesh was converted into vts/vtm files and further on into plot3D files, in order to process this mesh with Numeca IGG.

Coarse Mesh The coarse mesh was only used within Numeca simulations as part of a study about the influence of different turbulence models. Furthermore it was used to investigate the influence of heat transfer with the help of CHT simulations.

This block structured fluid mesh is quite coarse with 240k cells. Only 16 cells make up the diffuser mesh in radial direction. However it was very time-consuming to create the block structured solid mesh for the hub, because both mesh regions have to match at the hub, precisely the boundary curves of both hub patches. Thereby every time a new fluid mesh is created, which can be accomplished quite quickly, also a new solid mesh needs to be generated, which can take a very long time.

Solid Meshes Solid meshes are a rough approximation of the real geometry, especially regarding the backside, since no detailed technical drawings are available. Impeller and shaft were modelled as one part. Detailed mechanical gearing between impeller and shaft were not taken into account. Only different heat conductivities were specified for these two different solid parts, corresponding to the different materials. The Numeca solid mesh generated by Enzi [6] consists of 102k hexahedron cells, while the OpenFOAM mesh totals 84k tetrahedron cells.

Whereas the OpenFOAM solid mesh consists of a single continuous mesh, the Numeca solid mesh is split into blade mesh and hub mesh. On the one hand, this split mesh has the advantage that both parts can be created independently as block structured meshes. On the other hand, interpolation from the solid hub mesh to the fluid mesh as well as onto the solid blade mesh is necessary, which could lead to problems.

Since the OpenFOAM solid mesh is generated from unstructured tetrahedrons with Netgen [7], it can be refined in areas of greater significance, while coarsening it in other areas. The solid mesh resolution of the blade in Numeca is very fine because of the identical mesh resolution of the fluid mesh at the tip gap, which was extended down through the blade. This way the temperature gradients can be captured more precisely. The OpenFOAM blade mesh has a fine resolution only at the leading edge, and consists of only two cells along the blade thickness in the remaining areas. Nevertheless this should be sufficient for the temperature distribution.

The hub cell size in the OpenFOAM mesh is almost constant, whereas the Numeca mesh features great variances. This is due to the fact that the block structured approach keeps the cell number constant, for example in circumferential direction, although the radius varies considerably. The spinner mesh becomes finer and the impeller outlet becomes coarser this way.

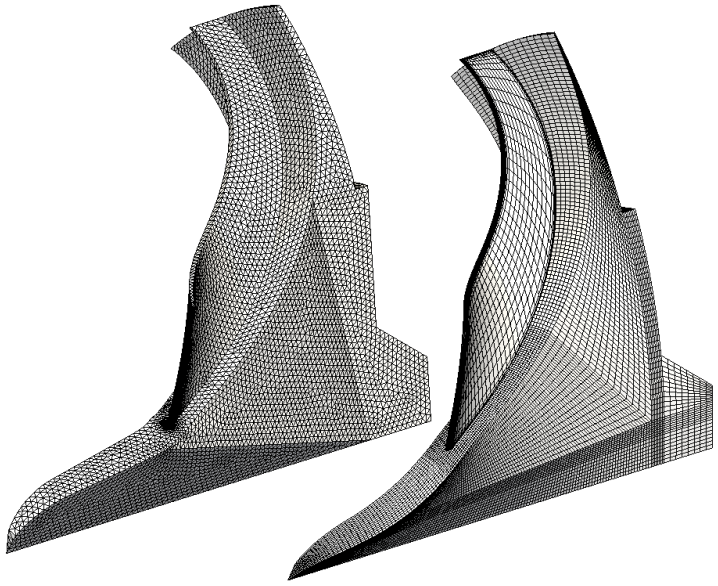

Figure 2. OpenFOAM (left) and Numeca (right) meshes of the solid impeller

Boundary Conditions

The stage was simulated using the frozen rotor approach, which means that there is no relative mesh motion between impeller and vaneless diffuser and the complete mesh is not rotating. Furthermore the flow is interpolated directly between both rows, thus the simulations could be made as steady state.

The simulations were performed on operating points at 80% design speed. Air was used as fluid and considered as perfect gas with $c_p = 1004.5\ J/(kg\ K)$ and $\varkappa = 1.4$. The laminar viscosity was modelled temperature dependent by the law of Sutherland.

Contrary to the experiments, the calculations were conducted at ISA inlet conditions. This approach has the advantage that all CFD results, meaning all fields, are already normed. In this way they can be directly analyzed without further conversion, which is convenient for larger mesh sizes. Tab. 1 shows the inlet boundary conditions for all computations. Solid walls are of no-slip type and adiabatic, except in the case of the CHT simulations for the fluid-solid patches. A constant temperature of 300 K was specified at the backside of the solid impeller, which led to an internal cooling of the impeller.

In Numeca one needs to specify k and ε even in the case of k-ω turbulence models. k and ε were chosen in a manner so that a

parameter	value
$p_{t,abs}$	101300 Pa
$T_{t,abs}$	288.15 K
$\vec{c}/\lvert\vec{c}\rvert$	$(0,0,1)$
ν_t	0.0001 $\frac{m^2}{s}$

Table 1. Fluid inlet boundary conditions

consistent turbulent viscosity is reached for the Spalart-Allmaras simulations. A turbulence intensity of 5% was assumed at the inlet for k. For the OpenFOAM calculations the turbulence intensity could be specified directly as boundary condition. This boundary condition adapts k for each inlet face during the calculation. In the case of the operating point P1 near the surge line the averaged values from the OpenFOAM case are $k = 30\ \frac{m^2}{s^2}$ and $\omega = 20000\ \frac{1}{s}$, and were prescribed for the Numeca computation. In OpenFOAM a special wall treatment is applied for first cells with $y^+ \gtrsim 11$, elsewhere the turbulence model acts as a low Reynolds number model. The way Numeca treats the walls can not be determined.

A constant static pressure was specified at the outlet, so that the massflow adjusts according to the experiments, with an error of about $\pm 1\%$. The solid heat conductivity λ was prescribed as listed in Tab. 2.

parameter	value
λ_{shaft}	$45[\frac{\text{W}}{\text{mK}}]$
$\lambda_{\text{impeller}}$	$50[\frac{\text{W}}{\text{mK}}]$

Table 2. Boundary conditions for heat transfer

Results

Overview CFD Simulations

Seven different CFD setups with two different mesh sizes at three different operating points each were investigated. Tab. 3 lists the experimental measured massflows for each operating point. An overview of the performed CFD simulations with the used turbulence model, mesh size and simulation type is given in Tab. 4. The simulations of the coarse Numeca mesh were performed by Enzi [6].

operating point	P1	M	S1
$\dot{m}_{red}\ [kg/s]$	1.82064	1.98646	2.30677

Table 3. Experimental massflows

Solver	Turbulence Model	Simulation	Mesh
Numeca	SA	Fluid	Coarse
Numeca	SA	CHT	Coarse
Numeca	SST	Fluid	Coarse
Numeca	SST	CHT	Coarse
Numeca	SST	Fluid	Fine
OpenFOAM	SST	Fluid	Fine
OpenFOAM	SST	CHT	Fine

Table 4. CFD simulations

The experimental raw data from Ziegler [1] were reprocessed, either as vtu files for the contour plots or as averaged values in spanwise and circumferential direction.

Global Data

In order to obtain global data from the CFD results, the primitive variables were averaged in a consistent manner to the experiments.

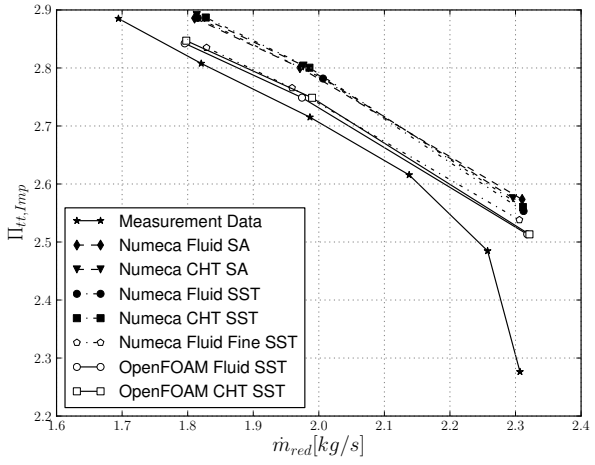

Figure 3. Impeller compressor map

The compressor map for the impeller is shown in Fig. 3. The total pressure ratio was computed in the CFD from the in-

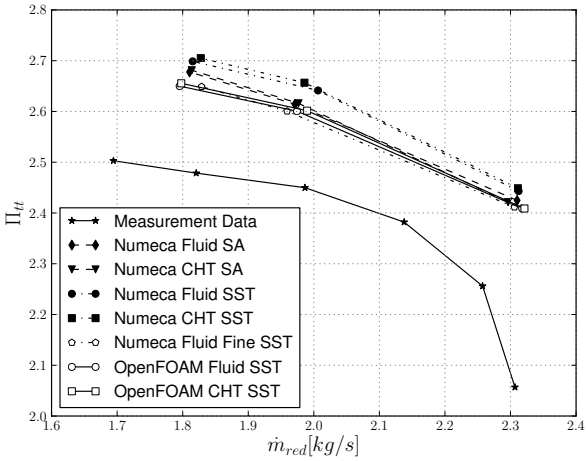

Figure 4. Stage compressor map

let to position 2M, whilst in the experiments the inlet duct was additionally present. All CFD results show in general a good accordance to the experimental data. Especially the slopes between the operating points P1 and M were captured well.

A too large choke massflow is predicted in all simulations. Thus the total pressure ratio is greater at the same massflow rate in S1. This might be partially caused by the simplified geometry modelling. For example the fillet between the hub and blade surface was not modelled. The fillet radius at the trailing edge is about 23% of the blade height.

As already explained, the CFD simulations were conducted at ISA conditions, while the experiments were done in the closed loop test rig. The experimental inlet conditions were approximately $p_{t,abs} = 60400\ Pa$ and $T_{t,abs} = 295.075\ K$. This results in a twice as high Reynolds number in the CFD simulations compared to the experiments. The compressor map is only Mach number independent. As already reported for example by Schäffler [8], the characteristic curves will shift slightly to the upper right of the compressor map for a higher Reynolds number. This effect might explain the constant offset which is apparent between the experimental and CFD results.

In both codes there is almost no difference between different turbulence models or simulation types regarding the impeller map. Only the mesh size effects the offset between experiment and CFD results. The coarse mesh predicts a higher total pressure ratio as the fine mesh in all operating points.

In Fig. 4 the compressor map of the complete stage is shown. In this case the outlet measurement position is 8M at a radius of $r_{8M} = 335\ mm$, close to the outlet of the vaneless diffuser. The slope is well captured by all simulations. Nevertheless the offset between measurements and CFD results increases, compared to the impeller map. The decrease of total pressure inside the vaneless diffuser is underpredicted in all CFD results, which might be attributed to the fact that the mixing losses of the impeller outflow were not well captured with the turbulence models. This outflow is locally highly turbulent and has strong gradients in spanwise and in circumferential direction. That makes it challenging to resolve all flow phenomena within an statistical approach. The Spalart-Allmaras turbulence model shows larger losses compared to the k-ω SST model with the coarse mesh. The fine mesh predicts a larger loss compared to the coarse grid, as it can resolve the flow phenomena more precisely.

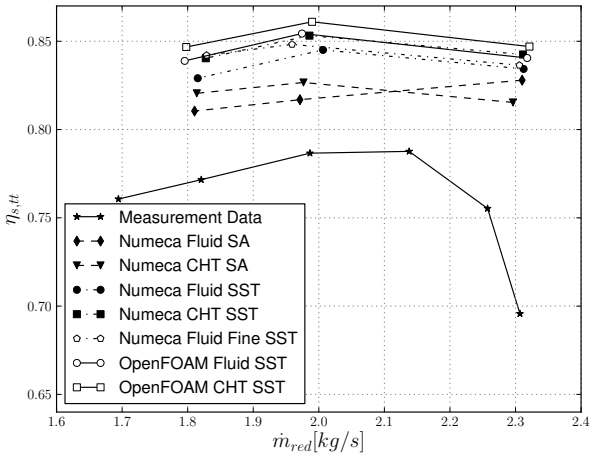

Figure 5. Isentropic total-total efficiency map

The isentropic total-total efficiency of the stage is plotted in Fig. 5. The trend of the efficiency characteristic, with a peak efficiency near the M operating point, is captured within almost all simulations. The CHT results show a higher efficiency compared to the simulations with adiabatic walls. That has to be the case, as there is a heat loss across the impeller due to the heat transfer, which decreases the outlet temperature, and therefore increases the efficiency at almost constant total pressure ratio. It should be pointed out that the Spalart-Allmaras S1 fluid simulation shows a higher efficiency as the CHT counterpart. Also the slope is not correctly predicted for this simulation. Due to the internal cooling of the CHT simulations, the density increases slightly, which furthermore increases the massflow at constant outlet pressure.

The comparison of the CFD results with the experimental data has shown in general a good accordance, especially in the case of the impeller. The influence of turbulence model and simulation type on the global data are almost negligible.

Measurement Position 2M'

A more detailed view of the flow topology inside the impeller was examined at the operating point near the surge line P1. The shown experimental data are L2F measurements at measure position 2M' shortly before the trailing edge of the impeller. They are compared to the corresponding fluid simulations on the fine grid of OpenFOAM and Numeca. The measurement window of the L2F experiments is smaller than the blade channel. This window is also shown as black border in the CFD results for a better orientation. Additionally the blades are drafted in all plots. It should be noted that these drafts do not show the fillets that are present in the real impeller.

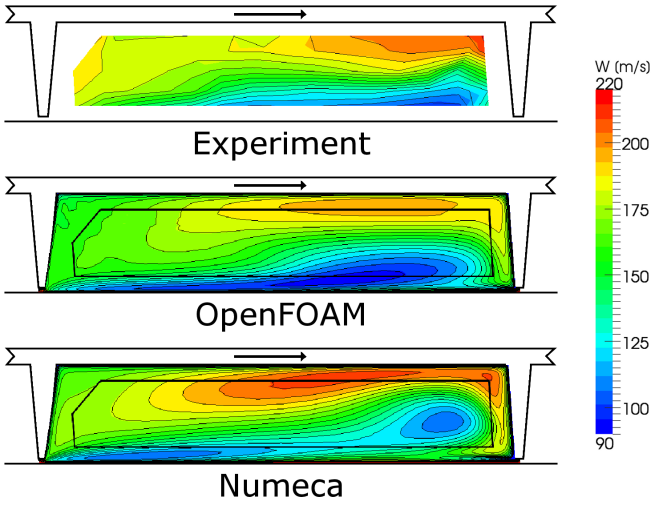

Figure 6. Relative flow velocity at position 2M'

In Fig. 6 the magnitude of the relative velocity is shown. This magnitude was computed with the velocity component perpendicular to the measurement surface and the relative circumferential velocity component, in order to be consistent with the experimental data. The relative velocity is a good parameter of the flow topology inside a centrifugal impeller. It is an indication of low and high momentum fluid inside the flow channel. Near the shroud and in the corner of shroud and suction side a region with low velocity is formed. This is called the wake region. On the pressure side and near the hub, high momentum flow is present, the jet region. The formation of this jet-wake-region is widely described in the literature, see for example Ziegler [1].

The experimental data also show such regions. The division line between these two is clearly visible between the pressure side - shroud corner and the suction side - hub corner. The OpenFOAM result is able to capture the jet wake region very well inside the measurement window. Solely close to the pressure side the jet is underpredicted. The division line between the jet-wake region is also predicted well.

The Numeca result clearly overpredicts the wake region. This minimum area is furthermore expanded from the shroud to the mid channel. This leads to an overprediction of the jet region. Thus the division line is also shifted slightly to the suction side.

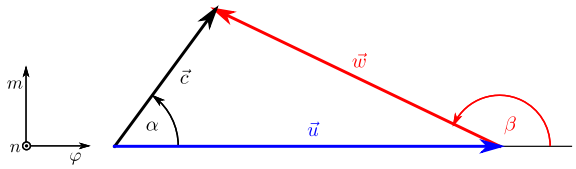

Figure 7. Angle definition

For the sake of completeness the definition of velocity angles is shown in Fig. 7.

The relative flow angle is plotted in Fig. 8. There is a region of slightly higher flow angle near the hub in the center of the blade channel. A region of lower relative angle with two minimum areas is present at about 30% span height.

In general the relative flow angle distribution is captured well by both CFD codes inside the measurement window. The minimum area of flow angle between pressure side and channel center is reproduced by both CFD codes. The OpenFOAM result predicts the location well, while the area in the Numeca result is shifted slightly to the pressure side. The second minimum near the suction side is not predicted in that occurrence by either simulations, this was already reported by Weiss [2].

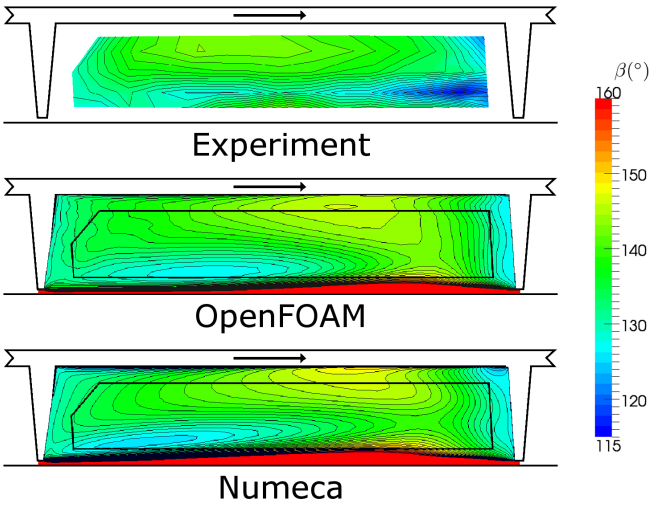

Figure 8. Relative flow angle 2M'

There is reverse flow directly near the shroud. In this region the radial velocity component becomes negative and thus the relative flow angle exceeds 180°. This behaviour was reported in the literature and was also shown by Weiss [2].

Turbulence Intensity The intensity of turbulence Tu for three dimensional flows can be written with the definition of the turbulent kinetic energy k as follows:

$$Tu = \frac{\sqrt{\frac{1}{3}\left(\overline{(c'_x)^2} + \overline{(c'_y)^2} + \overline{(c'_z)^2}\right)}}{|\vec{c}|} = \frac{\sqrt{\frac{2}{3}k}}{|\vec{c}|} \tag{1}$$

Unfortunately only two components of the absolute velocity vector were measured in the experiments, the transversal and longitudinal component inside the measurement plane. Thus only two components of the fluctuation velocities $\overline{(c')^2}$ are known. Ziegler [1] defined the two dimensional turbulence intensity as follows:

$$Tu^* = \sqrt{\frac{\frac{1}{2}\left(\overline{(c'_t)^2} + \overline{(c'_l)^2}\right)}{(\overline{c_t})^2 + (\overline{c_l})^2}} = \frac{\sqrt{\frac{1}{2}\left(\overline{(c'_t)^2} + \overline{(c'_l)^2}\right)}}{|\overline{\vec{c}_{tl}}|} \approx \frac{\sqrt{k}}{|\vec{c}|} \tag{2}$$

In the case of the measurement positions 2M and 2M' the difference between $|\vec{c}|$ and $|\overline{\vec{c}_{tl}}|$ is below 0.1%. Therefore it is assumed that also the fluctuations in the third direction are negligible. In that case both definitions can be linked together:

$$Tu = \sqrt{\frac{2}{3}}Tu^* \tag{3}$$

In Fig. 9 the corrected turbulence intensity is shown. There is a region of higher turbulence intensity near the shroud, caused by the non-rotating shroud. The gradient of turbulence intensity from the pressure side to the mid channel is well reproduced by both CFD codes. Nevertheless the Numeca result shows a larger peak area in the mid channel than the experiments. Also the OpenFOAM result slightly overpredicts the value in that area, but underpredicts it near the shroud.

Measurement Position 2M

Averaging procedure Spanwise and circumferentially averaged variables are shown in Fig. 10, Fig. 12 and Fig. 14.

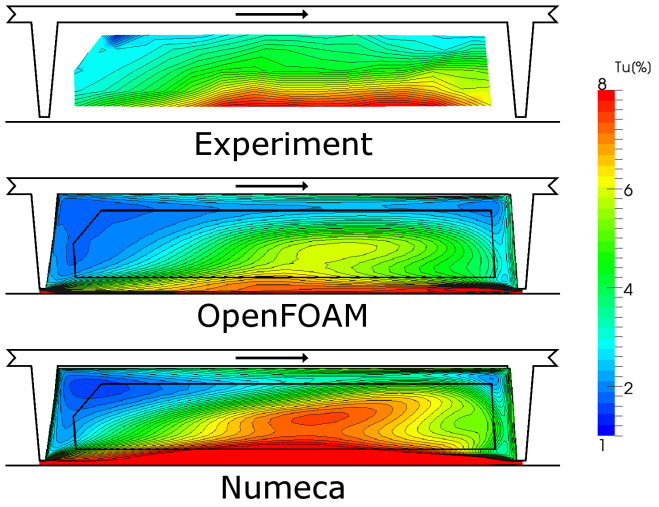

Figure 9. Turbulence intensity 2M'

These variables are based on L2F measurements in the case of experimental results. The corresponding plots are Fig. 11, Fig. 13 and Fig. 15. The circumferential as well as the spanwise averaging procedure at the measurement positions can be described with the following formula:

$$\bar{x} = \frac{\sum x_i \, c_{r,i} \, A_i}{\sum c_{r,i} \, A_i} \tag{4}$$

It is not possible to do a massflow weighted averaging of experimental data, as no density was measured. Therefore only the radial velocity component, which is perpendicular to the measurement surface 2M, was chosen as additional weighting factor. All plots are averaged with the same procedure in order to make sure the results are comparable. In the case of the CFD results virtual probes are used, in order to evaluate the flow variables, at the same locations as in the experiments.

The definition of the corresponding face area to each probe point was not defined precisely by Ziegler [1]. The distribution of probe points in spanwise direction is not equidistant. In order to make sure every probe point is the center of a virtual quad face, so that the data is representative for this face, the corresponding spanwise length to each probe position was determined, as shown in Tab. 5. The dimensionless span is defined from shroud ($z/b = 0$) to hub ($z/b = 1$), and the dimensionless circumferential

z/b	0.15	0.3	0.5	0.7	0.85
spanwise length [mm]	0.1	0.2	0.2	0.2	0.1

Table 5. Lentgh distribution

direction from the pressure side ($\phi/\phi_{pitch,Imp} = 0$) to the suction side ($\phi/\phi_{pitch,Imp} = 1$).

The weighting length distribution has only influence on the spanwise averaging. Other distributions with the same restriction are also possible, but this one seemed to be the most reasonable. The L2F probe distribution in the circumferential direction of the 2M section is equidistant. Thus the constant $\Delta\phi_i$ between two adjacent probe points has no influence on the circumferentially averaged value.

Furthermore no reference point was defined as starting point for the relative circumferential distribution $\phi/\phi_{pitch,Imp}$. This definition is necessary as the trailing edge is not infinitely thin. In this work the corner of the pressure side, trailing edge and tip surface was chosen. The starting point in circumferential direction $\phi/\phi_{\text{pitch,Imp}} = 0$ at measurement section 2M was swept back from the reference point about 1.775° for the numerical probes. This value was computed with Eq. 7.3 from Ziegler [1]. This position is held constant for all numerical post-processing. Nevertheless there is still a small uncertainty about the correct azimuthal position of the numerical probe points.

In Fig. 10, Fig. 12 and Fig. 14 the spanwise averages (left plot) and the circumferential averages (right plot) at position 2M for the P1 operating point are plotted. The averages from the experiments are from the L2F measurements, where $|\vec{c}|$, α and Tu were measured. All other variables were computed with the corresponding kinematic relationship. In each plot the averaged data from the experiments is compared to the CFD simulations.

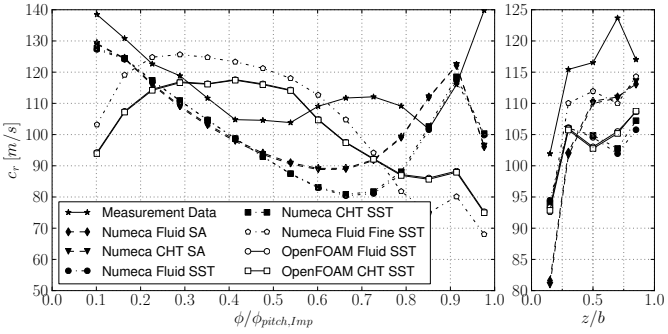

Figure 10. Averaged radial velocity

The averaged radial velocity component c_r is shown in Fig. 10. The Numeca results of the coarse mesh have a good accordance in the spanwise average from the pressure side to the mid channel. Unfortunately they cannot capture the constant level of radial velocity in the mid channel, instead c_r is underpredicted. Contrary to that the Numeca and OpenFOAM values of the fine mesh underpredict the radial velocity component at the pressure side. The simulations of the fine mesh show a positive slope first, contrary to the measurements, before they pass over to a negative one on the suction side. The minimum is located at the correct position in contrast to the coarse mesh. The velocity gradient at the suction side is captured only partially.

All CFD simulations show a good agreement of the circumferential averages. Only the Numeca SST results have a slightly negative slope in the mid channel, where an increase should be apparent. The lower velocity of the experimental data for the hub seems to be an averaging problem, as there is one probe point less which can be seen in Fig. 11, where a high radial velocity would be expected. There is almost no difference of the averaged plots between the CHT and fluid only simulations.

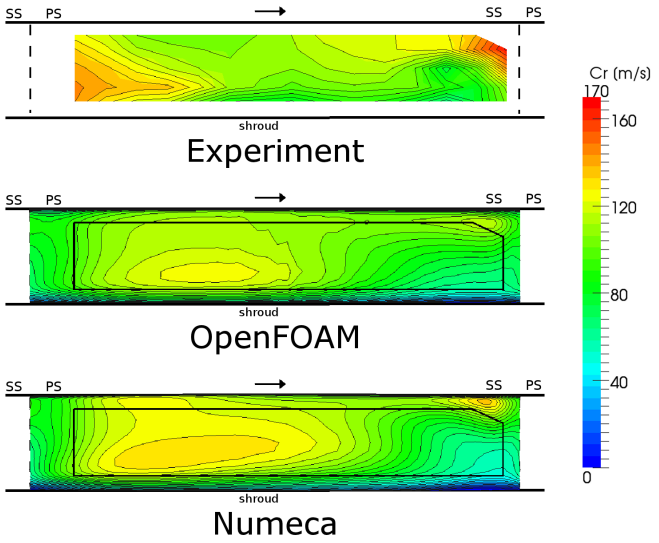

Figure 11. Radial velocity

In Fig. 11 the contour plots of the experimental data and the CFD results of the fine mesh are shown. The low velocity at the shroud is indicated in both CFD results. Both simulations are very similar. Nevertheless the predicted radial velocity level is lower, especially the maximum peak in the corner hub and suction side. The area of higher velocity is shifted in both cases to the mid channel. In the Numeca result the spanwise extension of higher radial velocity is larger. The CFD results show a minimum peak of the radial velocity in the corner of suction side and shroud. These aspects are in good agreement with the experiments.

As shown in Fig. 12 the OpenFOAM and Numeca results of the circumferential velocity for the fine mesh are conform with the experiments from the pressure side to the mid channel. The velocity minimum is underpredicted and shifted to the suction side, but the slope towards the suction side is predicted correctly.

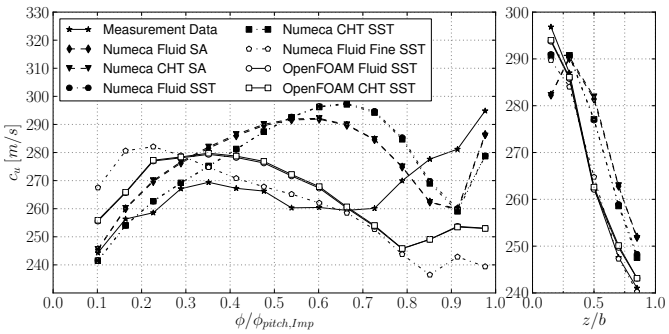

Figure 12. Averaged absolute circumferential velocity

The Numeca results of the coarse mesh have only a good shape in the first third part from the pressure side. The velocity component is clearly overpredicted in the mid channel. The value for the velocity minimum is reproduced well but it is shifted too close to the suction side.

The circumferentially averaged velocity is almost perfectly matched for the results of the fine mesh. Just the velocity near the shroud is slightly underpredicted, this is due to the too small velocity minimum. The Numeca circumferential averages of the coarse mesh have a positive offset, as this velocity component is predicted too high for a wide range, as also shown for the spanwise averages.

In Fig. 13 the contour plots of the absolute circumferential velocity c_u is plotted. The velocity distribution is divided into two parts again, a higher area at the shroud and region with lower velocity at the hub. This is in agreement with the magnitude

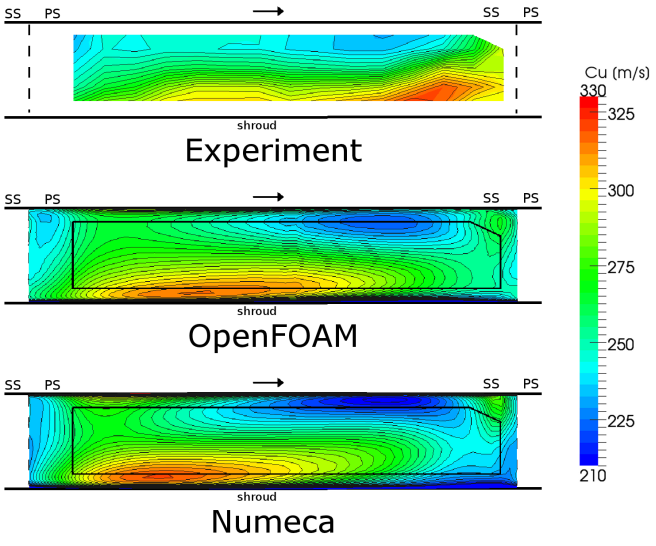

Figure 13. Absolute circumferential velocity c_u

of the relative velocity in section 2M' and the formation of the jet-wake structure inside the impeller. The reason for the very low relative velocity angle in the experiments near the suction side and shroud, which is plotted in Fig. 8, is the locally high circumferential velocity in this region. Both CFD results are not able to capture this area of locally high circumferential velocity. The occurrence of the wake region, and thus the circumferential velocity distribution, is highly influenced by the tip clearance, as already reported by Weiss [2]. Unfortunately no experimental data of the tip gaps at different operating conditions exists. Thus only results from a FE simulation are available.

Both CFD results are very similar and predict the circumferential velocity very well. They slightly underpredict the minimum value near the hub. The peak area near the suction side is not distinctive. The maximum at the shroud is shifted slightly towards the pressure side.

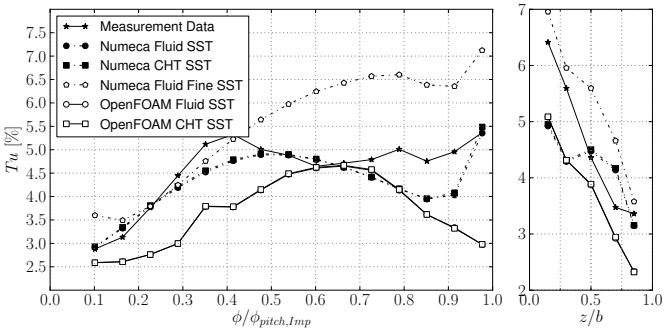

Figure 14. Averaged turbulence intensity

The averaged turbulence intensity is plotted in Fig. 14. The general characteristic of the spanwise averaged turbulence intensity is well met up until the mid channel for the Numeca result with the coarse mesh. The pressure side slope of the fine mesh from the Numeca result is reproduced quite well. The turbulence level is highly overpredicted in the mid channel. The location of the minimum as well as the slope at the suction side however is in agreement with the experiments. There is a shift of the OpenFOAM peak towards the suction side and the positive slope at the suction side is not visible. This is because of the lower turbulence prediction behind the trailing edge compared to the Numeca result, as can be seen in Fig. 15.

The circumferentially averaged slopes from the fine meshes of both CFD codes are similar. There is an offset of about 1.5%. The experimental averaged data is between these two results.

The maximum intensity of turbulence inside the measurement window near the shroud is underpredicted in both CFD results. The pressure side slope as well as the area of larger intensity in the mid channel is predicted fine with OpenFOAM and

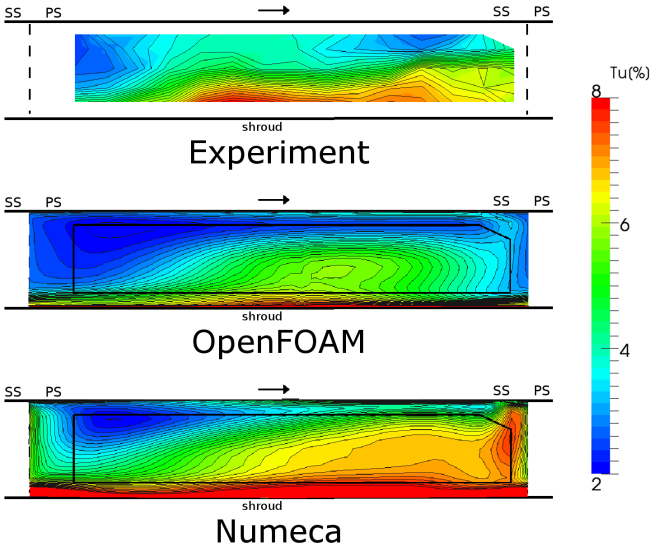

Figure 15. Turbulence intensity 2M

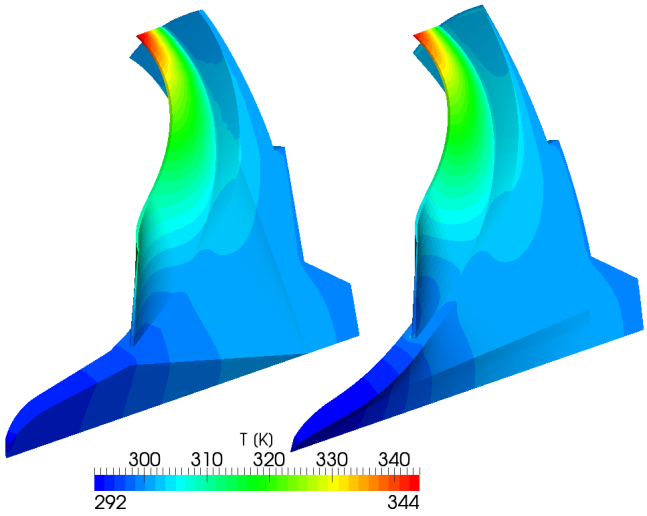

Figure 16. OpenFOAM (left) and Numeca (right) solid temperature distribution P1

Numeca, but the suction side turbulence is not met well by either code. The Numeca result shows a much higher level of turbulence intensity inside the wake region.

Solid Temperature Distribution

Additional time for CHT computation is almost not measurable in the OpenFOAM case. First and foremost this is due because the solid mesh size is just about 5% of the fluid mesh. Additionally only one scalar conservation equation has to be solved inside the solid, instead of a coupled set of conservation equations in the fluid region. As this is done in a fully implicit manner, no stability limitations for the time step are applied in the case of the OpenFOAM simulations. Unfortunately there is no comparable data available for the Numeca simulations.

Both CFD codes show in general similar temperature distributions as can be seen in Fig. 16. On the left hand side the OpenFOAM result is shown and on the right hand side the Numeca one. The small differences can be attributed to the different meshes, especially for the blade. Due to the relatively small total pressure ratio of this centrifugal compressor the temperature rise inside the impeller is only about 50 K. It should be pointed out, that Numeca applies an additional interpolation at the hub, which slightly distorts the temperature distribution. There are no significant differences in the temperature distributions between different operating points.

CONCLUSION

Numeca and OpenFOAM simulations of the RADIVER impeller have been conducted and compared to experimental data. It was shown that the CHT simulations have a minor influence on the flow topology in this case. Only the efficiency is predicted higher than with the fluid simulations. This was to be expected, because of the heat transfer from the fluid to the solid. As there is almost no additional computational cost for the CHT simulations, these should be used to predict the temperature distribution inside the solid impeller. This information is of great importance for structural analysis, especially for centrifugal compressors with a larger total pressure ratio.

The compressor map, especially the impeller map, has a good accordance with the measurements for all operating points. However, there is still a lack of accuracy predicting the diffuser flow. This can be attributed to the limits of the turbulence models regarding the mixing of the jet-wake flow.

There is a significant difference in flow details when comparing results from meshes with different resolutions. Coarse meshes did not capture the flow as well. Nevertheless they show only negligible variation in the compressor map. For detailed flow analysis finer fluid meshes were used, which achieved a very good similarity to the experiments. The circumferential averages in particular were met very well. Most characteristic flow patterns were reproduced reliably, but still not all flow details could be resolved.

It should be noted that there are still some uncertainties, like the size of the rotor gap, which have a great influence on the detailed flow topology. Thus it is hard to do an accurate comparison between experiments and CFD simulations.

REFERENCES

[1] Ziegler, K. U. M., 2003. "Experimentelle Untersuchung der Laufrad-Diffusor-Interaktion in einem Radialverdichter variabler Geometrie". PhD Thesis, Rheinisch-Westfälische Technische Hochschule Aachen.

[2] Weiß, C. H.-G., 2002. "Numerische Simulation der reibungsbehafteten Strömung in Laufrädern von Radialverdichtern". PhD Thesis, Rheinisch-Westfälische Technische Hochschule Aachen.

[3] Boncinelli, P., Ermini, M., Bartolacci, S., and Arnone, A., 2007. "On Effects Of Impeller Interaction In The 'RADIVER' Centrifugal Compressor". In ASME Turbo Expo: Power for Land, Sea and Air, no. GT2007-27384.

[4] Smirnov, P. E., Hansen, T., and Menter, F. R., 2007. "Numerical Simulation Of Turbulent Flows In Centrifugal Compressor Stages With Different Radial Gaps". In ASME Turbo Expo: Power for Land, Sea and Air, no. GT2007-27376.

[5] Borm, O., Jemcov, A., and Kau, H.-P., 2011. "Density Based Navier Stokes Solver for Transonic Flows". In 6th OpenFOAM Workshop, PennState University, USA.

[6] Enzi, D., 2010. "Simulation des Wärmetransfers in einem Radialverdicher". Semester thesis, Institute for Flight Propulsion, Technische Universität München.

[7] netgen, 2011. Version 4.9.13. `http://sourceforge.net/projects/netgen-mesher`.

[8] Schäffler, A., 1980. "Experimental and Analytical Investigation of the Effects of Reynolds Number and Blade Surface Roughness on Multistage Axial Flow Compressors". *ASME Journal of Engineering for Power,* ***102***, pp. 5–12.